ARTICLE   OPEN

Intensification of Arabian Sea cyclone genesis potential and its association with Warm Arctic Cold Eurasia pattern

P. J. Vidya [ID][1 ✉], Sourav Chatterjee[1], M. Ravichandran[2], S. Gautham[3], M. Nuncio[1] and R. Murtugudde[4,5]

The present study examines the drivers of the observed increasing trend in the Genesis Potential Index (GPI) of the post-monsoon season (October-November-December) tropical cyclones in the Arabian Sea (AS) during the period, 1998–2021. The increase in atmospheric moisture loading, ocean heat content in the upper 300 m (OHC300) and reduction in vertical wind shear are the major factors which caused the intensification in cyclone GPI in the recent decades. The increase in atmospheric moisture loading and OHC300 are consistent with the overall observed ocean warming trend of the region. However, the reduction in vertical wind shear has resulted from an anomalous large-scale upper atmospheric anticyclonic circulation over central India. Further investigation shows a concurrent transition of the Warm Arctic Cold Eurasia (WACE) pattern to its positive phase which strengthened and shifted the Subtropical Jet (STJ) poleward. This resulted in the anticyclonic circulation anomaly and altered the upper tropospheric zonal winds over the AS cyclone genesis region, weakening the vertical wind shear. The study demonstrates a possible physical mechanism through which remote forcing due to changes in the northern high-latitude climate can influence the AS cyclone genesis.

INTRODUCTION

Tropical cyclones (TCs) are one of the most devastating natural hazards which develop over the warm oceans (typically sea surface temperature (SST) >26 °C). Warming of the northern Indian Ocean (NIO) in recent decades supports the increase in the frequency of cyclones and their rapid intensification[1]. The AS has experienced dramatic surface (1.2–1.4 °C) and subsurface (1.4 °C)[2] warmings in recent years[3] compared to earlier decades[4]. This enhanced warming is likely enhancing the convective activity over the AS, which favours the formation and intensification of the TCs in recent decades[5]. The cyclone rapid intensification rate in the NIO is much higher (38%) than in the northwest Pacific Ocean (22%)[4].

The AS cyclone contribution to the annual global frequency of the cyclones is only 2% but the loss of life tends to be disproportionately high[4]. Through the transport of heat from the ocean to the atmosphere, the increase in SST favours an increase in the tropical cyclone intensity[6]. It can lead to extreme sea level and wind-wave conditions and change the upper ocean characteristics[7]. Yu and Wang (2009)[8] showed that the 4.6% increase in the TC potential intensity over the AS region is due to global warming. The strongest cyclone in the AS thus far was Cyclone Gonu, with maximum wind speeds of 240 km/h (150 mph, super cyclonic or category 5), which occurred on 1–8 June 2007 (India Meteorological Department (IMD)), caused 50 deaths and about $4.2 billion in damage in Oman, and ~$215 million in damage in Iran[9]. The second strongest cyclone in the AS is Cyclone Kyaar, a super cyclonic or category 4 cyclone (150 mph, IMD) that occurred from 24 October to 03 November 2019[10].

TCs are strongly coupled systems involving atmospheric and oceanic feedbacks throughout their life cycle. The most important oceanic and atmospheric parameters influencing the cyclogenesis in the Indian Ocean are SST, relative humidity, potential instability, vertical wind shear, relative/absolute vorticity and vertical velocity[11]. In general, cyclogenesis in the ocean is tracked and predicted using the Genesis Potential Index (GPI) based on dynamic and thermodynamic atmospheric circumstances[12]. Several studies[13–15] have explored different GPI formulations to define TC genesis indices. They have also tested the GPI's ability to represent the real pattern of TCs. IMD uses the GPI (relative vorticity, relative humidity, vertical wind shear and thermal instability) developed by Kotal et al. (2009)[12] to identify the potential areas of cyclogenesis over NIO with a few days lead time[11]. Since ocean parameters like SST and ocean heat content play an important role in cyclone genesis and its intensification, later Zhang et al. (2016)[16] developed a new GPI index using both atmosphere and ocean parameters.

The factors influencing the GPI may both be local or remote. For example, the large-scale ocean-atmosphere conditions such as the Maddan-Julian Oscillation (MJO), El Niño Southern Oscillation (ENSO), and Indian Ocean Dipole (IOD) influence the frequency and intensity of tropical cyclones in the NIO. According to a study by Krishnamohan et al. (2012)[17], the MJO fosters the most favourable conditions for cyclogenesis and its intensification in the NIO. According to study by Girishkumar et al. (2015)[18] and Pan & Li. (2008)[19], TCs are more frequent and rapidly intensify over the Bay of Bengal during La Niña and negative IOD periods than they are during El Niño or positive IOD period.

However, the potential of extratropical atmospheric circulations to influence the NIO TCs are not well explored. It is known that the changes in the mid- and high-latitude atmospheric circulations can influence the NIO through interactions among tropical and extratropical climate modes[20] or through mid-latitude Rossby wave trains guided by changes in the subtropical and polar jets[21]. The tracks of the TCs over the NIO can also potentially be guided by the alteration in the steering winds due to large-scale circulation changes[22,23]. Pan and Li. (2008)[19] showed that the mid-latitude perturbations propagate southward in the form of a Rossby wave, and the signals originating from western Europe can

[1]National Centre for Polar and Ocean Research (NCPOR), Ministry of Earth Sciences, Headland Sada, Goa 403 804, India. [2]Ministry of Earth Sciences (MoES), Prithvi Bhavan, Lodhi Road, New Delhi 110003, India. [3]CSIR-National Institute of Oceanography, Dona Paula, Goa 403004, India. [4]Inter-Disciplinary Program in Climate Studies, Indian Institute of Technology, Bombay, India. [5]ESSIC/AOSC, University of Maryland, College Park, USA. ✉email: vidya@ncpor.res.in
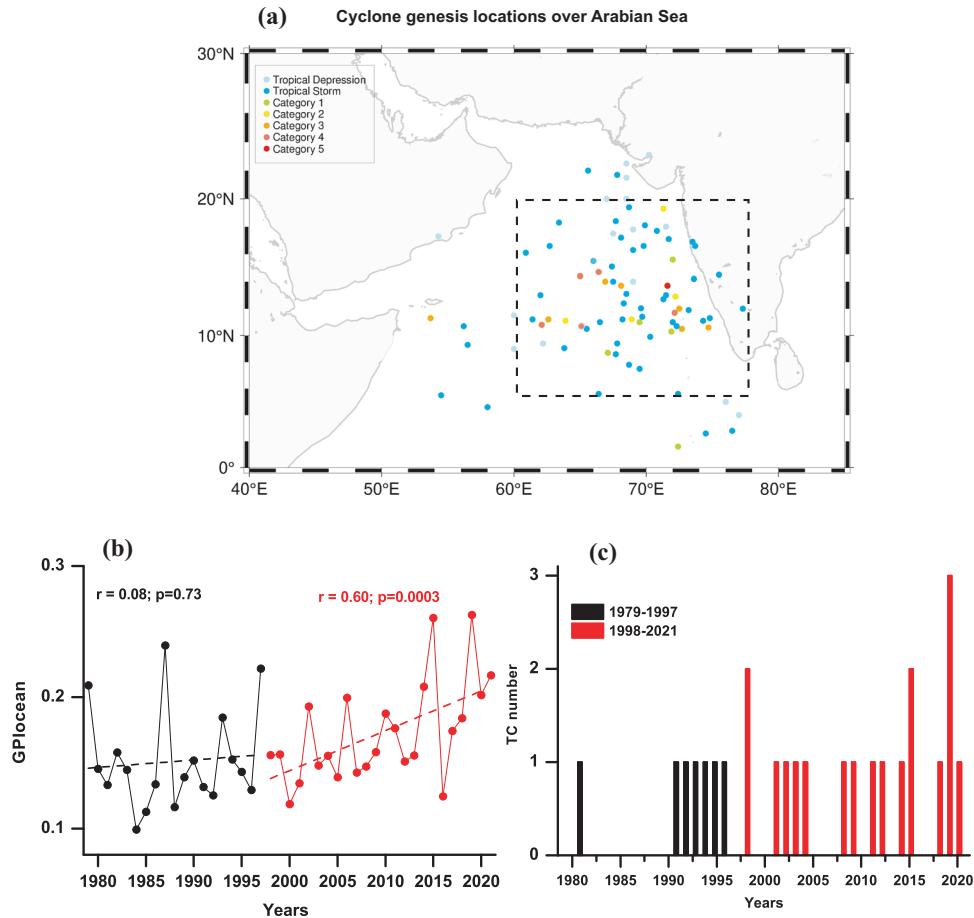
Fig. 1 Tropical Cyclones (TC) in the Arabian Sea and its changes during 1979–1997 and 1998–2021. a TC genesis locations in the AS, (**b**)TC Genesis Potential Index (GPI) during post-monsoon season (October-November-December; OND) from 1979 to 2021, (**c**) Number of cyclones (Depressions are not included) in the AS during the post-monsoon season. The black dash box in (**a**) indicates the TC genesis region (60–78°E & 5–20°N) while the filled colours indicate the intensity (category) of the TC. The dashed black and red lines in (**b**) indicate the trend lines and 'r' and 'p' indicate the regression slope and its significance, respectively, in each period. *p* values are computed using the student's two-tailed *t*-test.

reach the tropical Indian Ocean within 7 days. On interannual timescales, North Atlantic Oscillation is known to influence atmospheric circulation over the AS during the winter months (JFM)[21]. A recent study by Chen et al. (2023)[24] showed that the winter Arctic Sea Ice concentration anomaly is a potential predictor for the frequency of TC genesis in the western North Pacific during the following summer. However, it is not well explored if the rapidly warming Arctic[25] has any remote influence on intensifying TCs over the NIO or AS as well.

Here in this study, we investigate the changes in TCs properties over the AS for 1979–2021 using the GPI provided by Zhang et al. (2016)[16]. We then investigate the potential causes of this positive trend during this period after the regime shift (1998–2021)[26,27] in light of the significant increasing trend in the GPI since the climate regime shift in the Pacific SST pattern identified in 1996–97[28]. Further, a possible mechanism through which the changes in the atmospheric circulation patterns in the mid- and high-latitudes in the backdrop of rapid warming in the Arctic can explain the observed intensification of the TCs in the AS is investigated.

RESULTS AND DISCUSSION
TC genesis in the AS
Figure 1a displays the locations of the cyclone genesis in the AS (60–78°E & 5–20°N). Though, TCs occur in the pre-monsoon and

post-monsoon seasons (Supplementary Fig. 1), we focused only on the post-monsoon TCs for the current investigation. In the AS, the TC GPI, displays a significant increasing trend since 1998 during the post-monsoon season. However, GPI trend was not significant during 1979–1997 (Fig. 1b). Consistent with this, the number of TCs and their frequency have also increased since 1998 compared to previous period (Fig. 1c, *t* value $= -1.774$, $p = 0.04$)). We also computed the maximum possible surface winds that a TC could attain called Cyclone Maximum Potential Intensity (MPI) followed by Emanuel (1987)[29] and Walsh (2019)[30]. Mean MPI showed higher values in the cyclogenesis region (Supplementary Fig. 2a). Constitent with this, spatial trend of the MPI also show significant positive values in the cyclogenes region (Supplementary Fig. 2b). Since, both GPI and MPI showed increasing trend during 1998–2021 in the cyclogeneis region, we consider only GPI for the further study. To decipher the causes, we have analysed the important factors that can influence the cyclone GPI in the AS. As the GPI trend is significant, only during 1998–2021, further analyses focus only on this period.

Factors controlling TC genesis in the AS
The moisture content in the atmosphere plays a vital role in the TC development, and moisture loading and its locations of moisture perturbations are also essential for the intensification of TCs[31]. All the atmospheric and oceanic parameters are averaged over the TC
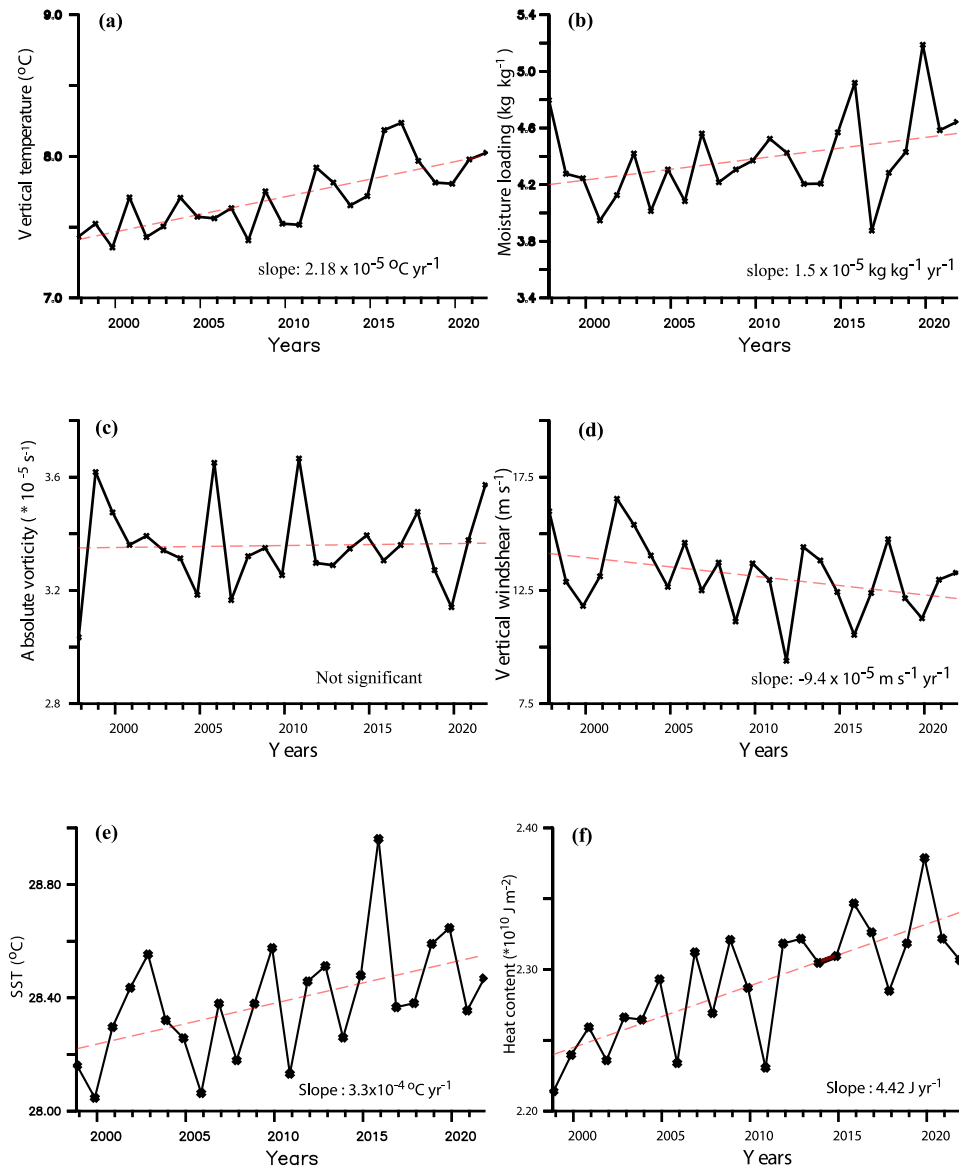
Fig. 2 Trends in atmospheric and oceanic factors associated with GPI. Post-monsoon timeseries of (**a**) vertically averaged temperature in the atmosphere (1000–500 hPa), (**b**) vertically integrated (1000–500 hPa) moisture load in the atmosphere, (**c**) absolute vorticity at 1000 hPa, (**d**) vertical wind shear, (**e**) SST and (**f**) ocean heat content in the upper 300 m (OHC300). The red dashed lines indicate the trend lines. The trends are significant above 95% confidence level except for the absolute vorticity (**c**). All the figures are averaged over TC genesis region (60–78°E & 5–20°N). p values are computed using the student's two-tailed t-test.

genesis region shown in Fig. 1a (60–78°E & 5–20°N). Vertically averaged (1000 hPa–500 hPa) atmospheric temperature (Fig. 2a, $p = 0.00003$) and vertically integrated moisture loading (humidity) (Fig. 2b, $p = 0.009$) show a significant increasing trend during the study period (1998–2021). Moisture loading and atmospheric temperature (1000 hPa–500 hPa) show a higher correlation outside the cyclogenesis region (Supplementary Fig. 3a). Moisture loading shows a strong correlation with SST in the cyclogenesis region (Supplementary Fig. 3b). It indicates that the warming of the ocean provides more moisture to the atmosphere, which can contribute to the formation and strengthening of TCs. As warmer ocean (higher SST) evaporates more easily, and can lead to more condensation heating with cloud formation and convection. A strong positive correlation between SST and air temperature at 2 m further confirms the role of SST towards the increase in moisture loading in the atmosphere (Supplementary Fig. 3c). The absolute vorticity (Fig. 2c, $p = 0.7$) has not experienced any significant trend, while vertical wind shear (Fig. 2d, $p = -0.01$)

shows a significant decreasing trend. Consistent with the increase in atmospheric temperature, the oceanic factors such as SST (Fig. 2e, $p = 0.01$) and OHC300 (Fig. 2f, $p = 0.00002$) also show a significant increasing trend during the post-monsoon season. All the p values are computed using the student's two-tailed t-test. Increase in SST and OHC300 help to intensify the TC by the sustained supply of heat fluxes to the atmosphere[6]. Thus, the increasing GPI and increased number of cyclones during this period are likely due to synergistic oceanic (SST, OHC300) and the atmospheric factors (vertical wind shear and moisture loading). In the AS, the increase in atmospheric temperature, moisture loading and OHC300 during the post-monsoon season are due to anthropogenic warming in the recent decades[32]. Using CMIP5 model projections, Murakami et al. (2017)[32] also showed that increased anthropogenic aerosols in the lower troposphere can weaken the South Asian Winter Monsoon circulation and reduce the vertical wind shear over the AS during the post-monsoon season.
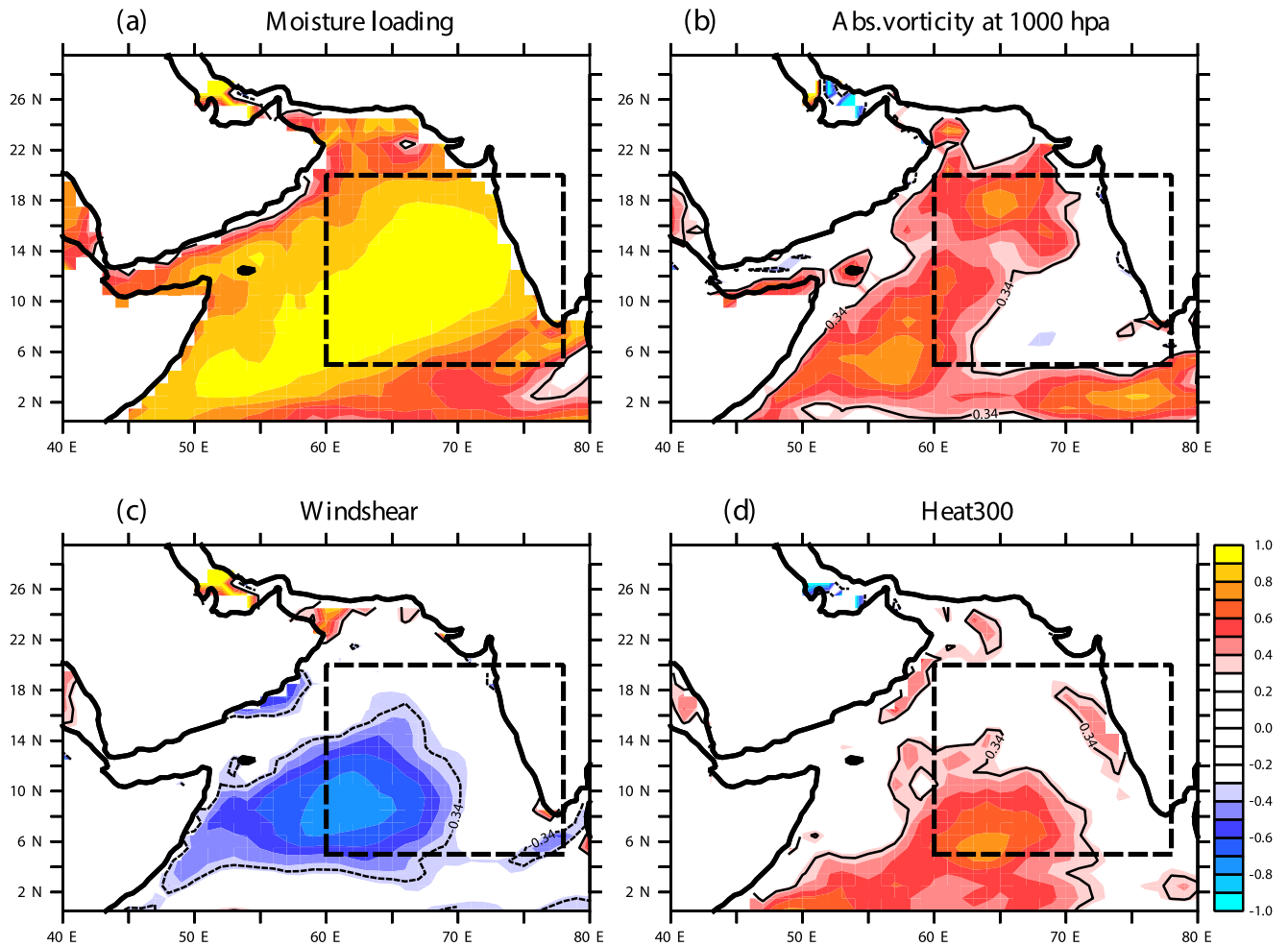
Fig. 3 **Correlation between GPI and associated atmospheric and oceanic factors.** Spatial correlation map during the post-monsoon mean GPI with (**a**) moisture loading (1000–500 hPa), (**b**) absolute vorticity, (**c**) vertical wind shear, and (**d**) OHC300m. The black dashed box indicates the TC region. Only significant values at 95% confidence level are shown. p values are computed using the student's two-tailed t test.

Spatial correlations between GPI and the associated parameters such as moisture loading (Fig. 3a), absolute vorticity (Fig. 3b), vertical wind shear (Fig. 3c), and OHC300 (Fig. 3d) were also computed to elicit their role in controlling GPI variability in the AS. Consistent with the trends (Fig. 2), vertically integrated moisture loading (Fig. 3a; $r \geq 0.9$, $p < 0.05$) and OHC300 (Fig. 3d; $r \geq 0.6$, $p < 0.05$) show significant correlations in the TC genesis region during the post-monsoon season, while the absolute vorticity (Fig. 3b, $P > 0.05$) does not show any significant correlation. In contrast, vertical wind shear shows a significant negative correlation (Fig. 3c, $P < 0.05$). Thus, these results indicate that both the trend and variability of GPI in the AS TC genesis region are driven by the increases in SST, OHC300, moisture loading and a reduction in vertical wind shear during this period. A comparison of the relative dependence of GPI in the AS on these three factors (SST, OHC300 and vertical wind shear) is shown in Fig. S4. Moisture loading, vertical wind shear, and OHC300 show correlation (>95% significance) values of 0.9, −0.35 and 0.6, respectively. Thus, while the oceanic factors are more strongly associated with the GPI trend, a statistically significant contribution from vertical wind shear is also observed in this period.

Vertical wind shear (either vertical or horizontal) between the low levels (850 hPa) and the upper levels (200 hPa) is an important parameter affecting TC formation and its intensification. Low vertical wind shear allows the storm to remain vertically aligned and strengthen the cyclonic circulation, while a large vertical wind shear can disrupt the cyclone formation. Figure 4a and b depict

the post-monsoon upper atmospheric circulation during the period 1979–1997 and 1998–2021, respectively. Figure 4c represents the difference in upper atmospheric circulation at 200 hPa between the period 1998–2021 and 1979–1997. The winds are southeasterly in the cyclogenesis region during both the periods (Fig. 4a and b). The difference between two periods (Fig. 4c) showed an anticyclonic circulation anomaly over central India (Fig. 4c). As a result, zonal winds (200 hPa) over the AS TC genesis region have become anomalous easterlies (the easterly component has intensified) after 1998 (Fig. 4c). The mean value of the zonal wind speed in the AS cyclone genesis region is $1.8 \, ms^{-1}$ for 1979–1997, and $-1 \, ms^{-1}$ for 1998–2021 (Fig. 4d). The mean wind patterns at 200 hPa and at 850 hPa (1979–2021) and their anomalies between the two periods (1998–2021 minus 1979–1997) are shown in Supplementary Fig. 4. These changes in the wind direction at 200 hPa and 850 hPa have resulted in a reduction of the vertical wind shear over the AS TC genesis region and has likely favoured the formation of intense TCs. In the next section, we investigate the change in large-scale circulation features and its role in controlling the vertical wind shear over the AS during this period.

A possible physical mechanism

To explore the possible remote influences on the increase in the intensity of the anticyclonic circulation above the AS region, we
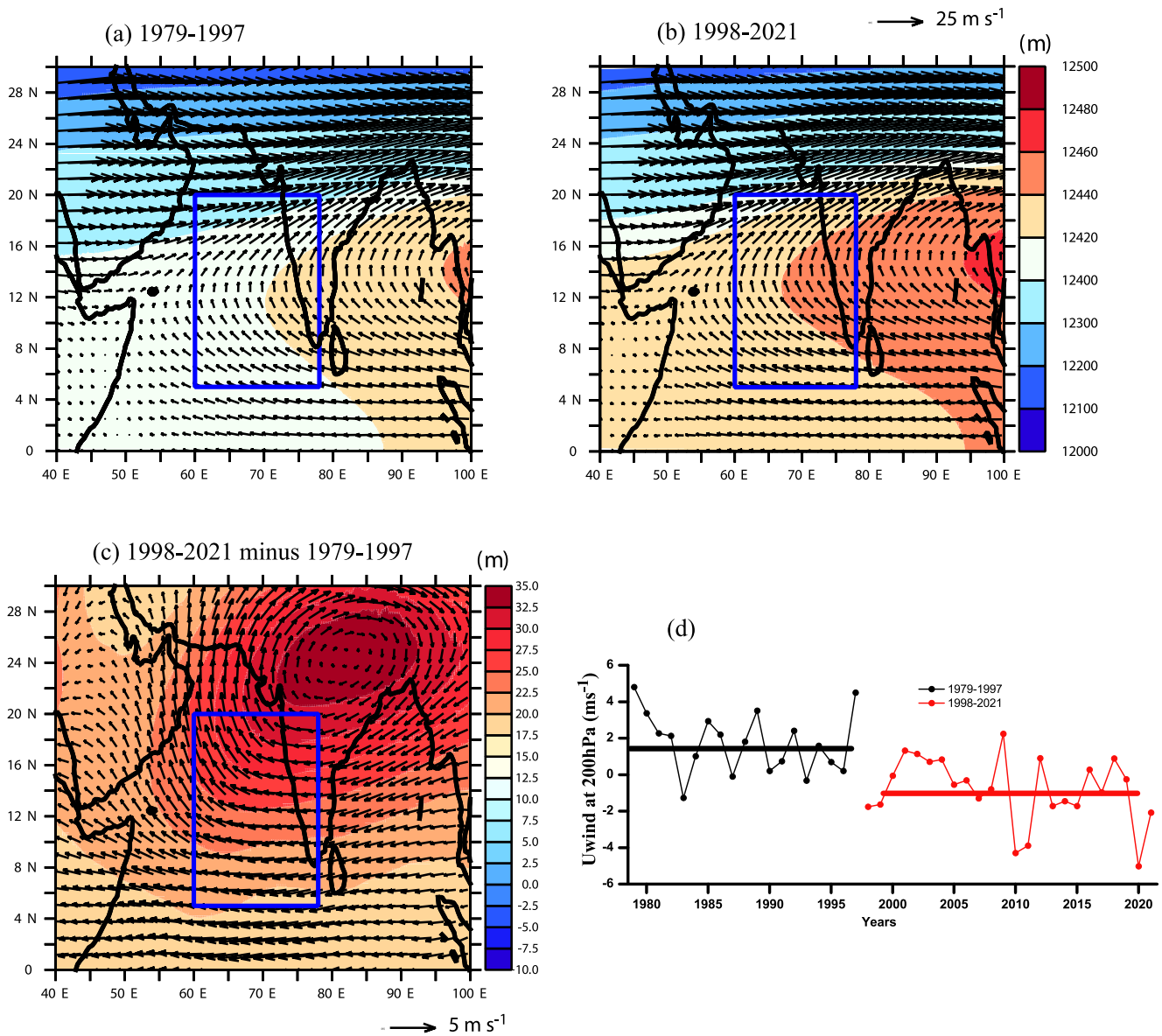
(a) 1979-1997

(b) 1998-2021

→ 25 m s⁻¹ (m)

(c) 1998-2021 minus 1979-1997 (m)

(d)

→ 5 m s⁻¹

Fig. 4 Upper atmospheric circulation changes associated with GPI. a Geopotential height (m) at 200 hPa averaged (**a**) 1979–1997, (**b**) 1998–2021, overlaid with winds at 200 hPa. **c** Difference between (**b**) and (**a**) overlaid with the wind anomaly at 200 hPa (The difference in geopotential height at 200 hPa between two periods are statistically significant at 95% confidence level). **d** Time series of zonal winds averaged over the TC genesis (60-78°E & 5-20°N) region. All the figures are averaged during post-monsoon season. *p* values are computed using the student's two-tailed *t* test.

investigated its interaction with mid-latitude circulation changes. One of the key features of the present-day mid-latitude climate is the Warm Arctic Cold Eurasia (WACE) pattern[33–35]. The WACE pattern is defined as the warming of the Arctic, along with frequent cold events in the northern hemisphere mid-latitudes over Eurasia. Several studies[34–36] have suggested that warming in the Barents-Kara Sea region of the Arctic Ocean is closely associated with this pattern which starts to develop from fall and becomes most prominent in winter. We formulate the WACE index by taking the difference in surface air temperature between the Barents-Kara Sea region and the central Eurasian region (Fig. 5a) during the fall, i.e. the post-monsoon season (OND). Interestingly, concurrent with the strengthening of anticyclonic circulation in the upper troposphere, a phase shift in the WACE index post-1998 can be noticed. The upper atmospheric circulation feature associated with the WACE pattern is obtained from a linear regression of this WACE index on the 200 hPa geopotential

heights (Fig. 5b). Consistent with earlier study of Lou et al. (2022)[37], positive height anomalies over the warm Barents-Kara Sea region and negative anomalies over central Asia are found to be associated with WACE.

The anomalous negative height anomalies over central Eurasia, in turn, strengthen the subtropical jet (STJ) over the Asian sector (Fig. 6a). As a result, with the strengthening of the dipole height anomalies between Barents-Kara Sea and central Eurasia after 1997, the STJ gets stronger to its poleward side (Fig. 6). This poleward strengthening of the STJ results in stronger positive meridional gradient in zonal winds (Fig. 7a) and induces negative relative vorticity over central India, strengthening it after 1997 (Fig. 7b). Thus in summary, the positive phase of WACE since around 1997 and the associated changes in the upper tropospheric circulation may have intensified the anticyclonic circulation by strengthening the STJ poleward. The schematic diagram depicting the above mechanism is shown in Fig. 8.
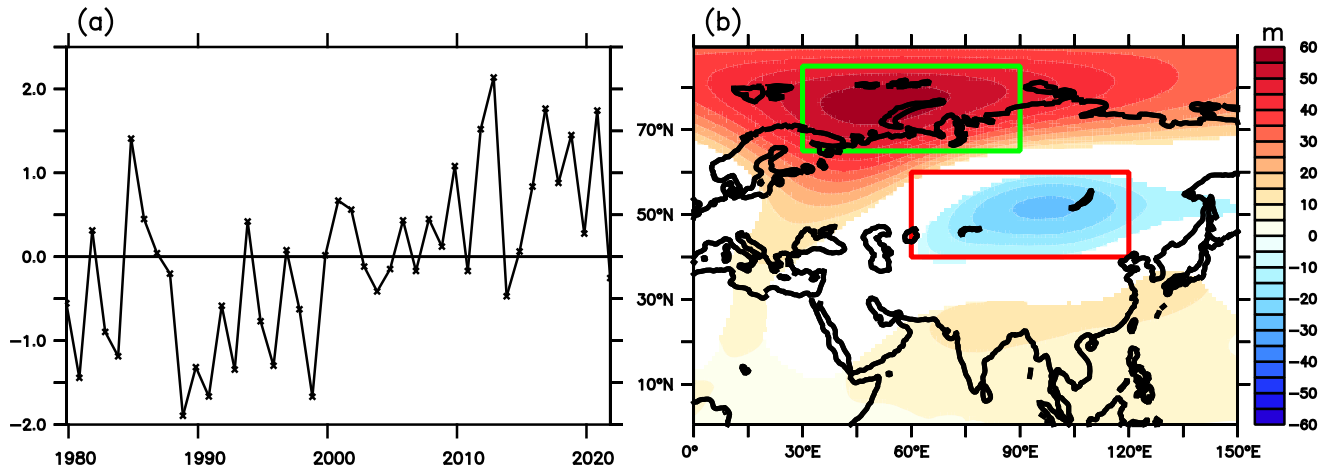
Fig. 5 Warm Arctic Cold Eurasia (WACE) pattern and associated upper atmospheric circulation. a Normalised time series of difference in surface air temperature (2 m) during the post-monsoon between Barents-Kara Sea region (30–90°E & 65–85°N) and central Eurasia (60–120°E & 40–60°N) as marked in (Fig **b**). **b** Regression of the timeseries in (**a**) on the post-monsoon geopotential height (m) at 200 hPa. Only significant values at 95% confidence level are shown in (**b**). p values are computed using the student's two-tailed t test.
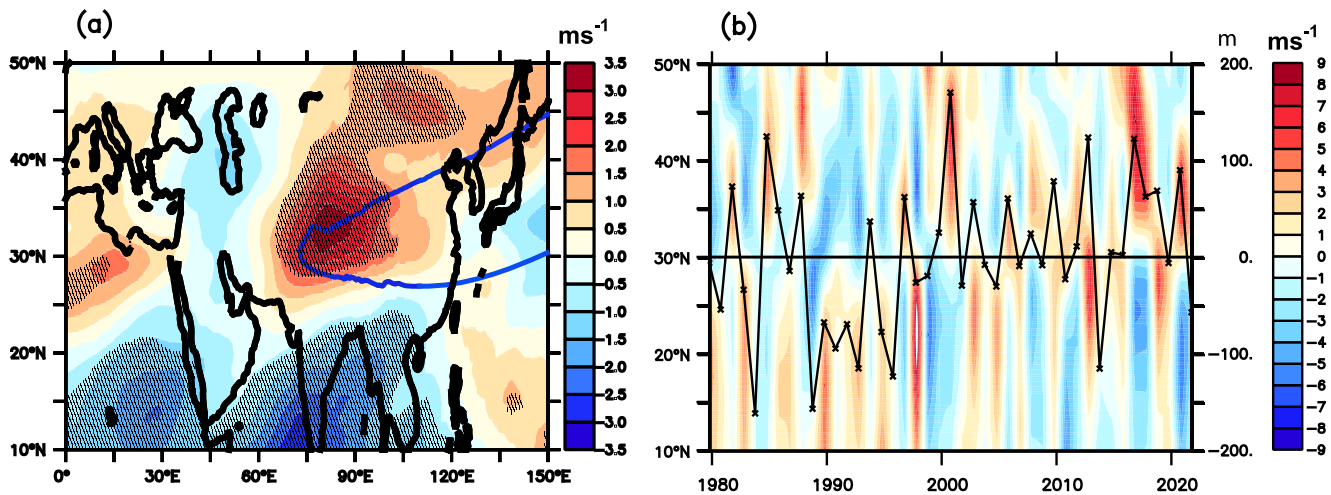
Fig. 6 Changes in Subtropical jet associated with WACE circulation pattern. a Averaged difference in the post-monsoon zonal winds (ms^{-1}) at 200 hPa between 1998–2021 and 1979–1997. Shading indicates a significant difference at 95% confidence level. The blue contour indicates the climatological (1979–2021) position of the jet stream core identified as the 40 ms^{-1} contour. **b** Latitude vs. time (Hovmoller) plot of the post-monsoon zonal winds (ms^{-1}) at 200 hPa averaged over 60°E–120°E. The timeseries (corresponding to the right Y axis) shows the difference in 200 hPa geopotential height between the Barents-Kara Sea region (30-90°E & 65-85°N) and central Eurasia (60-120°E & 40-60°N) as marked in 5b. p values in (**a**) are computed using the student's two-tailed t test.

The AS has undergone an increase in cyclone GPI from 1998 to 2021 during the post-monsoon season. Our analysis suggests that the increase in ocean and atmosphere warming and reduced vertical wind shear have led to the intensification of TC GPI. The weakening of the vertical wind shear is due to the strengthening of anticyclonic circulation over central India. Our study also shows that the recent positive phase of the WACE pattern since 1997 and the associated changes in the upper tropospheric circulation have intensified the anticyclonic circulation by strengthening the STJ on its poleward-side. Thus, we propose that the recent increase and intensification of TCs over the AS is at least partly driven by the remote teleconnections associated with the rapidly warming Arctic and its interaction with mid-latitude upper atmospheric circulation, providing favourable conditions for the TC intensification over the AS. With the climate models projecting more intense cyclones in the coming decades (IPCC AR6), further studies are needed for a quantitative estimate of the contribution from remote forcing to the AS TC numbers and intensity. It is virtually certain that there have been local feedbacks associated with the remote forcing as well, but these need further analysis, which will be reported elsewhere.

METHODS

Details of data used and sources

Monthly means of atmospheric variables such as geopotential height at 200 hPa, zonal and meridional winds, specific humidity, and atmospheric temperature with spatial resolution $0.25° \times 0.25°$ for the period January 1979–December 2021 are provided by the fifth generation ECMWF reanalysis (ERA5;[38]). Monthly means of oceanic factors such as SST, ocean potential temperature, and upper ocean heat content down to 300 m (OHC300) with spatial resolution $0.25° \times 0.25°$ for January 1979–December 2021 are obtained from ORAS5[38]. Both the atmospheric and oceanic data are taken from the source: https://cds.climate.copernicus.eu/cdsapp#!/dataset/.
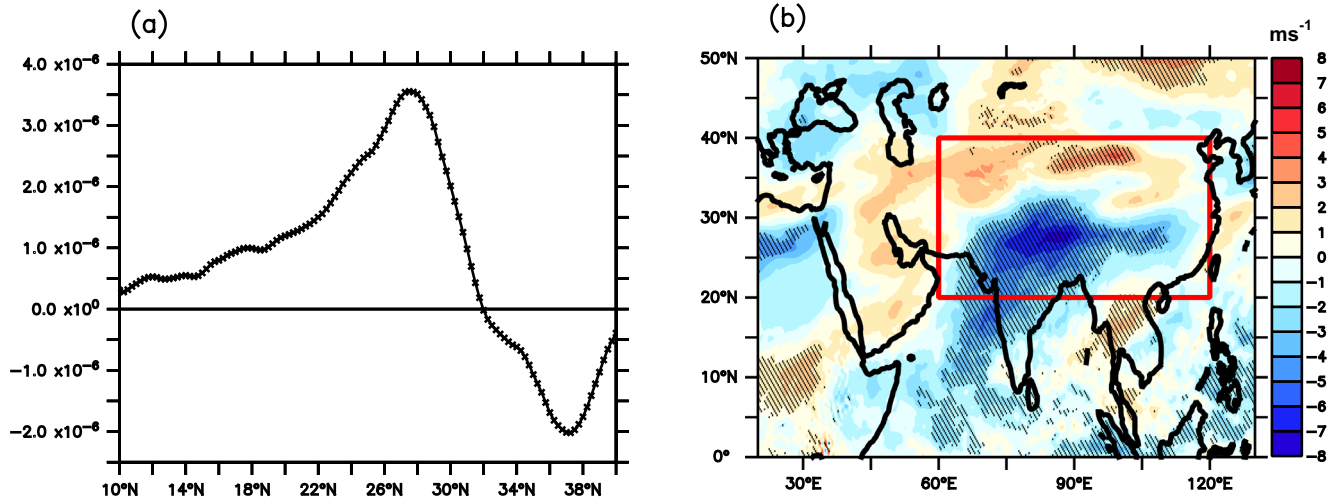
Fig. 7 Upper atmospheric circulation changes over central India. a Difference in meridional gradient (du/dy x10^{-6} s^{-1}) in 200 hPa zonal winds between 1998–2021 and 1979–1997, averaged over 60°E-120°E. **b** The difference in relative vorticity (10^{-6} s^{-1}) between 1998–2021 and 1979–1997. Shading indicates a significant difference at 95% confidence level. *p* values are computed using the student's two-tailed *t* test.
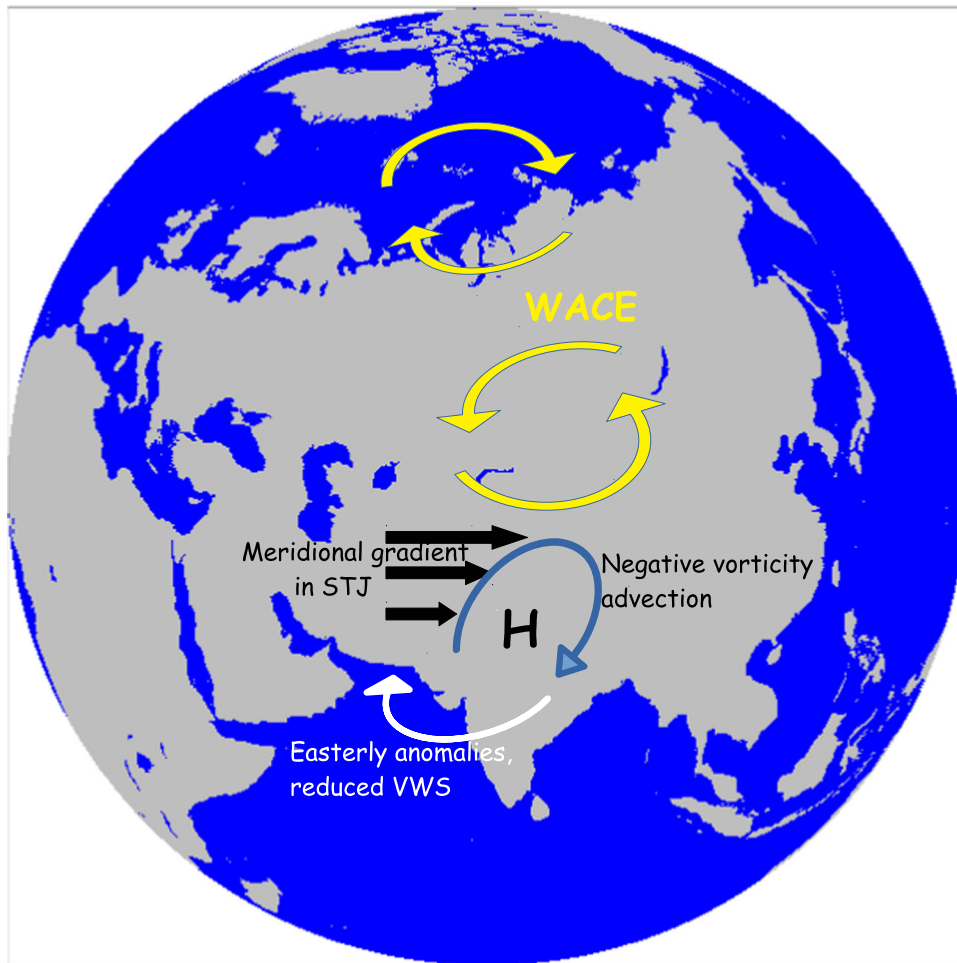

Fig. 8 Schematic diagram of a possible physical link between WACE and TC genesis in the Arabian Sea (AS). Upper atmospheric circulation changes associated with WACE strengthens the STJ poleward and induces a negative relative vorticity over central India. The resulting anomalous anticyclonic circulation strengthens the anomalous eaterly winds over AS and reduces the vertical wind shear (VWS) over the AS, favouring stronger GPI.

GPI computation

To re-emphasise, considering the rapid changes in AS oceanic environment, for a better representation of the oceanic influence on the TCs, the GPI is calculated as in[16] using the equation:

$$GPI_{ocean} = p|10^5\eta_{1000}|^{0.9}\left(\frac{\overline{T}}{26}\right)^{7.64}\left(\frac{F}{45}\right)^{-2.73}\left(\frac{D_{26}}{80}\right)^{0.25}, \quad (1)$$

Where, η_{1000} is the absolute vorticity at 1000 hPa, T is the average sea water temperature in the mixed layer, F is the net longwave radiation (W m^{-2}), and D26 is the depth of the 26 °C isotherm. The coefficient p enables the best least square fit between GPI_{ocean} and observations, and $p = 7.4 \times 10^{-3}$.

The absolute vorticity (η_{1000}) was calculated using the equation,

$$\eta_{1000} = \zeta + f, \quad (2)$$

Where ζ is the relative vorticity and f is the Coriolis parameter.

Vertical wind shear

Vertical wind shear is calculated based on the wind speed difference between 200 hPa and 850 hPa using the following equation:

$$Vertical\ Wind\ Shear\ (VWS) = \sqrt{(U_{200hPa} - U_{850hPa})^2 + (V_{200hPa} - V_{850hPa})^2} \quad (3)$$

Maximum potential intesity (MPI)

Cyclone Maximum Potential Intensity (MPI) is computed followed by Emanuel (1987)[29] is given by,

$$|V_{max}|^2 = \frac{C_k}{C_D}\frac{T_s - T_0}{T_0}\left(k_0^* - K\right) \quad (4)$$

Where T_s is the sea surface temperature and T_0 is the temperature near the tropopause (top of the TC). C_k and C_D are transfer coefficients of momentum and enthalpy. k_0^* and K are the specific enthalpies of ocean surface and air near the surface. Those values are estimated at the eyewall where winds are maximum. $\frac{C_k}{C_D}$ ratio is generally assumed to be 1 due to lack of measured values.

Cyclone track data

Tropical cyclone tracks and cyclone counts were taken from the International Best Track Archive for Climate Stewardship (IBTrACS;[39]) and the Cyclone eAtlas of the India Meteorological Department (IMD). Pre-monsoon April through early June and post-monsoon October through December are the two cyclone seasons in the NIO[4]. Significance of all the trends were tested with the student's two-tailed t test at 95% significance level.

REFERENCES

1. Vinodhkumar, B., Busireddy, N. K. R., Ankur, K., Nadimpalli, R. & Osuri, K. K. On occurrence of rapid intensification and rainfall changes in tropical cyclones over the North Indian Ocean. *Int. J. Climatol.* **42**, 714–726 (2022).
2. Sreenivas, P., Chowdary, J. S. & Gnanaseelan, C. Impact of tropical cyclones on the intensity and phase propagation of fall Wyrtki jets. *Geophys. Res. Lett.* **39**, 1–6 (2012).
3. Albert, J., Gulakaram, V. S., Vissa, N. K., Bhaskaran, P. K. & Dash, M. K. Recent Warming Trends in the Arabian Sea: Causative Factors and Physical Mechanisms. *Climate* **11**, 35 (2023).
4. Singh, V. K. & Roxy, M. K. A review of ocean-atmosphere interactions during tropical cyclones in the north Indian Ocean. *Earth-Sci. Rev.* **226**, 103967 (2022).
5. Sreenath, A. V., Abhilash, S., Vijaykumar, P. & Mapes, B. E. West coast India's rainfall is becoming more convective. *npj Clim. Atmos. Sci.* **5**, 1–7 (2022).
6. Emanuel, K. A. An air-sea interaction theory for tropical cyclones. *Part I: Steady-state Maint. J. Atmos. Sci.* **43**, 585–604 (1986).
7. Vissa, N. K., Satyanarayana, A. N. V. & Prasad Kumar, B. Response of Upper Ocean during passage of MALA cyclone utilizing ARGO data. *Int. J. Appl. Earth Obs. Geoinf.* **14**, 149–159 (2012).
8. Yu, J. & Wang, Y. Response of tropical cyclone potential intensity over the north Indian Ocean to global warming. *Geophys. Res. Lett.* **36**, 1–5 (2009).
9. Fritz, H. M., Blount, C. D., Albusaidi, F. B. & Al-Harthy, A. H. M. Cyclone Gonu storm surge in Oman. *Estuar. Coast. Shelf Sci.* **86**, 102–106 (2010).
10. Golshani, A., Banan-Dallalian, M., Shokatian-Beiragh, M., Samiee-Zenoozian, M. & Sadeghi-Esfahlan, S. Investigation of Waves Generated by Tropical Cyclone Kyarr in the Arabian Sea: An Application of ERA5 Reanalysis Wind Data. *Atmos.* **13**, 1914 (2022).
11. Suneeta, P. & Sadhuram, Y. Tropical cyclone genesis potential index for Bay of Bengal during peak post-monsoon (October-November) season including atmosphere-ocean parameters. *Mar. Geod.* **41**, 86–97 (2018).
12. Kotal, S. D., Kundu, P. K. & Roy Bhowmik, S. K. Analysis of cyclogenesis parameter for developing and nondeveloping low-pressure systems over the Indian Sea. *Nat. Hazards* **50**, 389–402 (2009).
13. George, J. E. & Gray, W. M. Tropical cyclone motion and surrounding parameter relationships. *J. Appl. Meteorol.* **15**, 1252–1264 (1976).
14. Emanuel, K. & Nolan, D. S. Tropical cyclone activity and the global climate system. In *26th Conference on Hurricanes and Tropical Meteorology, Miami, Fla. Am. Met. Soc.* **10A.2**, 240–241 (2004).
15. Tippett, M. K., Camargo, S. J. & Sobel, A. H. A poisson regression index for tropical cyclone genesis and the role of large-scale vorticity in genesis. *J. Clim.* **24**, 2335–2357 (2011).
16. Zhang, M., Zhou, L., Chen, D. & Wang, C. A genesis potential index for Western North Pacific tropical cyclones by using oceanic parameters. *J. Geophys. Res. Ocean.* **121**, 7176–7191 (2016).
17. Krishnamohan, K. S., Mohanakumar, K. & Joseph, P. V. The influence of Madden-Julian Oscillation in the genesis of North Indian Ocean tropical cyclones. *Theor. Appl. Climatol.* **109**, 271–282 (2012).
18. Girishkumar, M. S., Suprit, K., Vishnu, S., Prakash, V. P. T. & Ravichandran, M. The role of ENSO and MJO on rapid intensification of tropical cyclones in the Bay of Bengal during October–December. *Theor. Appl. Climatol.* **120**, 797–810 (2015).
19. Pan LL, L. T (2008). Interactions between the tropical ISO andmidlatitude low-frequency flow. *Clim. Dyn.* **31**, 375–388 (2008).
20. Zhou, S. & Miller, A. J. The interaction of the Madden-Julian oscillation and the Arctic oscillation. *J. Clim.* **18**, 143–159 (2005).
21. Gong, D. Y. et al. Interannual linkage between Arctic/North Atlantic Oscillation and tropical Indian Ocean precipitation during boreal winter. *Clim. Dyn.* **42**, 1007–1027 (2014).
22. Francis, D., Fonseca, R. & Nelli, N. Key Factors Modulating the Threat of the Arabian Sea's Tropical Cyclones to the Gulf Countries. *J. Geophys. Res. Atmos.* **127**, e2022JD036528 (2022).
23. Singh, V. K., Roxy, M. K. & Deshpande, M. Role of subtropical Rossby waves in governing the track of cyclones in the Bay of Bengal. *Q. J. R. Meteorol. Soc.* **148**, 3774–3787 (2022).
24. Chen, S. et al. Impact of the winter Arctic sea ice anomaly on the following summer tropical cyclone genesis frequency over the western North Pacific. *Clim. Dyn.* **61**, 3971–3988 (2023).
25. Rantanen, M. et al. The Arctic has warmed nearly four times faster than the globe since 1979. *Commun. Earth Environ.* **3**, 168 (2022).
26. Vidya, P. J. et al. Increased cyclone destruction potential in the Southern Indian Ocean. *Environ. Res. Lett.* **16**, 014027 (2020).
27. Wanson, K. L. & Tsonis, A. A. Has the climate recently shifted? *Geophys. Res. Lett.* **36**, L06711 (2009).
28. Hong, C. C., Wu, Y. K. & Li, T. Influence of climate regime shift on the interdecadal change in tropical cyclone activity over the Pacific Basin during the middle to late 1990s. *Clim. Dyn.* **47**, 2587–2600 (2016).
29. Emanuel, K. A. The dependence of hurricane intensity on climate. *Nature* **326**, 483–485 (1987).

30. Walsh, K. et al. Tropical cyclones and climaTe change. *Trop. Cyclone Res. Rev.* **8**, 240–250 (2019).

31. Wu, L. et al. Impact of environmental moisture on tropical cyclone intensification. *Atmos. Chem. Phys.* **15**, 14041–14053 (2015).

32. Murakami, H., Vecchi, G. A. & Underwood, S. Increasing frequency of extremely severe cyclonic storms over the Arabian Sea. *Nat. Clim. Chang. 2017 712* **7**, 885–889 (2017).

33. Kim, H.-J., Son, S.-W., Moon, W., Kug, J.-S. & Hwang, J. Subseasonal relationship between Arctic and Eurasian surface air temperature. *Sci. Rep.* **11**, 4081 (2021).

34. Cohen, J. et al. Recent Arctic amplification and extreme mid-latitude weather. *Nat. Geosci.* **7**, 627–637 (2014).

35. Overland, J. E., Wood, K. R. & Wang, M. Warm Arctic–cold continents: climate impacts of the newly open Arctic Sea. *Polar Res.* **30**, 15787 (2011).

36. Inoue, J., Hori, M. E. & Takaya, K. The role of barents sea ice in the wintertime cyclone track and emergence of a warm-Arctic cold-Siberian anomaly. *J. Clim.* **25**, 2561–2568 (2012).

37. Luo, B., Luo, D., Dai, A., Simmonds, I. & Wu, L. Decadal Variability of Winter Warm Arctic-Cold Eurasia Dipole Patterns Modulated by Pacific Decadal Oscillation and Atlantic Multidecadal Oscillation. *Earth's Futur.* **10**, e2021EF002351 (2022).

38. Hersbach, H. et al. The ERA5 global reanalysis. *Q. J. R. Meteorol. Soc.* **146**, 1999–2049 (2020).

39. Knapp, K. R., Kruk, M. C., Levinson, D. H., Diamond, H. J. & Neumann, C. J. The international best track archive for climate stewardship (IBTrACS). *Bull. Am. Meteorol. Soc.* **91**, 363–376 (2010).

AUTHOR CONTRIBUTIONS

Author P.J.V. conceived the idea with S.C. and R.M. P.J.V., S.C., M.R., S.G., N.M. and R.M. designed the analysis. All authors contributed to writing the paper.

COMPETING INTERESTS

The authors declare no competing interests.

ADDITIONAL INFORMATION

Supplementary information The online version contains supplementary material available at https://doi.org/10.1038/s41612-023-00476-2.

Correspondence and requests for materials should be addressed to P. J. Vidya.

Reprints and permission information is available at http://www.nature.com/reprints

Publisher's note Springer Nature remains neutral with regard to jurisdictional claims in published maps and institutional affiliations.